

Panoramic $H\alpha$ and mid-infrared mapping of star formation in a $z = 0.8$ cluster

Yusei Koyama^{1*}, Tadayuki Kodama², Kazuhiro Shimasaku^{1,3}, Masao Hayashi¹,
Sadanori Okamura^{1,3}, Ichi Tanaka⁴ and Chihiro Tokoku⁵

¹*Department of Astronomy, School of Science, The University of Tokyo, Tokyo 113-0033, Japan*

²*National Astronomical Observatory of Japan, Mitaka, Tokyo 181-8588, Japan*

³*Research Center for the Early Universe, School of Science, The University of Tokyo, Tokyo 113-0033, Japan*

⁴*Subaru Telescope, National Astronomical Observatory of Japan, 650 North A'ohoku Place, Hilo, HI 96720, USA*

⁵*Astronomical Institute, Tohoku University, Aramaki, Aoba-ku, Sendai, Miyagi 980-8578, Japan*

28 October 2018

ABSTRACT

We present the first wide-field $H\alpha$ imaging survey around the distant cluster RXJ1716.4+6708 at $z = 0.81$ with a narrow-band filter on MOIRCS/Subaru, which reveals the star formation activities down to a star formation rate (SFR) of $\sim 1 M_{\odot}/\text{yr}$ without extinction correction. Combining with a wide-field mid-infrared (MIR) imaging survey with AKARI satellite, we compare in detail the unobscured and obscured star formation activities in the cluster. We find that both $H\alpha$ emitters and MIR galaxies avoid the cluster central region and their spatial distribution is quite similar. Most of the $H\alpha$ emitters show blue colours, but we find some $H\alpha$ emitters on the red sequence. The MIR galaxies tend to be systematically redder than the $H\alpha$ emitters probably due to heavy dust extinction. Interestingly, the red $H\alpha$ emitters and the red MIR galaxies (i.e. dusty red galaxies) are most commonly seen in the medium-density environment such as cluster outskirts, groups and filaments, where optical colours of galaxies change. We investigate the amount of hidden star formation by calculating a ratio, $\text{SFR}(\text{IR})/\text{SFR}(H\alpha)$, and find that $A_{H\alpha}$ exceeds ~ 3 in extreme cases for actively star-forming galaxies with $\text{SFR}(\text{IR}) \gtrsim 20 M_{\odot}/\text{yr}$. It is notable that most of such very dusty galaxies with $A_{H\alpha} \gtrsim 3$ are also located in the medium-density environment. These findings suggest that dusty star formation is triggered in the in-fall region of the cluster, implying a probable link between galaxy transition and dusty star formation. We finally calculate the cluster total SFR and find that the cluster total SFR based on $H\alpha$ alone can be underestimated more than factor ~ 2 even after 1 mag extinction correction. We suggest that the mass-normalized cluster SFR rapidly declines since $z \sim 1$ following $\propto (1+z)^6$, although the uncertainty is still large.

Key words: galaxies: clusters: individual: RXJ1716.4+6708 — galaxies: evolution — large-scale structure of Universe.

1 INTRODUCTION

It is well known that properties of galaxies are strongly correlated with environment in the sense that galaxies in high-density environment tend to be red and have early-type morphology. This is first quantitatively noted by Dressler (1980) in nearby clusters, and many other studies have confirmed such correlations as well as extended them in redshift space (e.g. Postman & Geller 1984; Dressler et al. 1997; Goto et al. 2003; Postman et al. 2005). Recent large, intensive spectroscopic surveys for the local Universe show that star-forming activity is also a strong function of environment (e.g. Lewis et al. 2002; Gómez et al. 2003; Tanaka et al. 2004) in the sense that star-forming activity is weaker in the higher-density

environment. Cluster galaxies are in fact mostly red early-types with little on-going star formation at least in the local Universe. However, if we look at distant clusters, we can find many blue star-forming galaxies in cluster environment (the so-called Butcher-Oemler effect: Butcher & Oemler 1984). Therefore by observing distant clusters at various redshifts (i.e. clusters in the past Universe at various epochs) we should be able to identify when and how the activities of cluster galaxies are changed from blue star-forming populations to red quiescent ones.

The ‘hidden’ star forming galaxies in clusters are also key population to characterize the evolution of cluster galaxies. Recent mid-infrared (MIR) observations of distant clusters with space telescopes such as Spitzer and AKARI discovered many dusty galaxies in $z \gtrsim 0.5$ clusters (Geach et al. 2006; Marcillac et al. 2007; Bai et al. 2007; Saintonge, Tran, & Holden 2008; Koyama et al.

* E-mail: koyama@astron.s.u-tokyo.ac.jp

2008; Krick et al. 2009). Although the number of clusters studied in MIR is still small, Saintonge, Tran, & Holden (2008) showed the trend that the dusty star-forming population is more commonly seen in the more distant clusters (see also Haines et al. 2009b). Koyama et al. (2008) showed the possibility of environmental dependence in the fraction of dusty star-forming galaxies at $z \sim 0.8$, and suggested that the MIR activity is enhanced in the ‘medium-density’ environment such as cluster outskirts, groups and filaments, where galaxy colours sharply change from blue to red.

Another good tracer of star formation is optical emission lines from galaxies. In particular, $H\alpha$ line (6563Å) is considered to be one of the best star formation indicators, since it directly reflects the emission from HII region in the star-forming sites. Moreover, $H\alpha$ line is less affected by dust extinction or metallicity, compared to [OII] line which has been commonly used in the studies of distant galaxies. However, since $H\alpha$ line shifts to near-infrared (NIR) regime at $z \gtrsim 0.4$, it has been difficult to conduct a large $H\alpha$ study for $z \gtrsim 0.4$ clusters until recently. There are some $H\alpha$ studies for low- z clusters with optical spectroscopy (Couch et al. 2001; Balogh et al. 2002) and with narrow-band imaging (Balogh & Morris 2000; Kodama et al. 2004), but the number of known clusters studied in $H\alpha$ is really small. For distant clusters, Finn, Zaritsky, & McCarthy (2004) and Finn et al. (2005) conducted narrow-band $H\alpha$ imaging surveys for several $z \sim 0.7$ – 0.8 clusters in NIR. However, their field coverage is limited to the central regions of the clusters. As suggested in Koyama et al. (2008), cluster surrounding environment is likely to be the key environment for galaxy evolution, but such spatially extended regions have been much less explored mainly due to the limited field of view of NIR instruments.

It is thus ideal to observe distant clusters in both of the two major, but independent indicators of star formation, namely, $H\alpha$ and MIR, over a wide area from cluster cores to surrounding environments. It is also important to quantify any different views of star forming activities seen by the two different indicators. Mapping out dusty and non-dusty star formation activities in distant clusters may give us a clue to understand what is actually happening in the transition environments. In this paper, we present the first such wide-field $H\alpha$ imaging survey over the known structures including the central cluster RXJ1716.4+6708 at $z \sim 0.8$. Combining with the similarly wide-field MIR data of this cluster taken with AKARI, we also attempt to compare the $H\alpha$ and MIR views of the $z > 0.8$ cluster.

The RXJ1716.4+6708 cluster (hereafter RXJ1716) that we target in this paper is a rich and probably unvirialized cluster at $z = 0.81$. The cluster was first discovered in the ROSAT North Ecliptic Pole Survey (NEP; Henry et al. 1997). Optical spectroscopy was performed by Gioia et al. (1999) and 37 cluster members were identified. Using this spectroscopic sample, Gioia et al. (1999) determined the cluster redshift $z_{cl} = 0.809$ and the velocity dispersion $\sigma = 1522^{+215}_{-150}$ km s⁻¹. This velocity dispersion is relatively large for its rest-frame X-ray luminosity of $L_{bol} = 13.86 \pm 1.04 \times 10^{44}$ erg s⁻¹ and the temperature $kT = 6.8^{+1.0}_{-0.6}$ keV (Ettori et al. 2004). This indicates that this cluster is not virialized yet and in the process of active assembly. In fact, this cluster has a small subcluster or group to the northeast of the main cluster. The morphology of this cluster in a X-ray image elongates towards the direction of the subcluster (e.g. Jeltama et al. 2005). Koyama et al. (2007) performed a wide-field, multi-colour optical imaging of this cluster and discovered prominent large-scale structures penetrating the cluster core and the second group of this cluster towards the southwest of the cluster core, based on the photometric redshift

technique. The weak-lensing mass of this cluster is estimated to be $2.6 \pm 0.9 \times 10^{14} h^{-1} M_{\odot}$ (Clowe et al. 1998). This is consistent with the estimated mass based on the X-ray data in Ettori et al. (2004); $M_{tot} = 4.35 \pm 0.83 \times 10^{14} M_{\odot}$.

The structure of this paper is as follows. In Section 2, we summarize our optical, NIR and MIR data. In Section 3, we show the selection technique of $H\alpha$ emitters from cluster members. The derivation of $H\alpha$ -derived star-formation rates is shown in Section 4. We show the results and discussions from Section 5 to Section 8, and summarize our results in Section 9. Throughout this paper, we use $\Omega_M = 0.3$, $\Omega_{\Lambda} = 0.7$, and $H_0 = 70$ km s⁻¹Mpc⁻¹. Magnitudes are all given in the AB system.

2 DATA

2.1 Optical data

We use the optical data in Koyama et al. (2007). We performed deep and wide-field $VRiz'$ imaging of the RXJ1716 cluster with Suprime-Cam (Miyazaki et al. 2002) on the Subaru Telescope (Iye et al. 2004), as a part of the PISCES project (Panoramic Imaging and Spectroscopy of Cluster Evolution with Subaru; Kodama et al. 2005). A summary of the data and the method of data reduction is described in Koyama et al. (2007), and we just repeat some important points here.

We reduced the data using a pipeline software SDFRED (Yagi et al. 2002; Ouchi et al. 2004). Source detection and photometry were done using SExtractor software (Bertin & Arnouts 1996). We use 2'' aperture magnitudes (MAG_APER) for measuring galaxy colours and MAG_AUTO are used as total magnitudes of galaxies. Our optical catalogue was constructed for objects brighter than $z' = 24.9$ which corresponds to the 5σ detection limit in z' -band. For our use in this paper, we applied a small aperture correction to the aperture magnitudes. This is because the seeing size of our near-infrared (NIR) data is slightly larger ($0.89''$, see Section 2.2.1) than that of the optical images ($\sim 0.7''$). We smoothed our optical images to $0.89''$ and determined the correction value, but the correction is small (~ 0.02 mag). We estimated photometric redshifts (phot- z) for all the galaxies using the phot- z code of Kodama, Bell, & Bower (1999). We found that $> 90\%$ of spectroscopically confirmed members listed in Gioia et al. (1999) fall within the redshift range of $0.76 \leq z_{phot} \leq 0.83$ (see fig.2 of Koyama et al. 2007), and used this range to select member candidates.

2.2 Near-infrared(NIR) data

2.2.1 Observation and data reduction

We observed the RXJ1716 cluster in J and NB119 filter with MOIRCS on the Subaru Telescope (Ichikawa et al. 2006; Suzuki et al. 2008). The NB119 filter perfectly matches to $H\alpha$ lines at $z = 0.81$ (i.e., the redshift of our target cluster). In Fig. 1 we compare the velocity distribution of spectroscopically confirmed members listed in Gioia et al. (1999) with the NB119 filter response function. It clearly shows that we can detect more than $\sim 80\%$ of $H\alpha$ emitting members within the FWHM of the NB119 filter if they have the same velocity distribution as that of the spectroscopic members in Gioia et al. (1999) and if their $H\alpha$ EWs are larger than the threshold of our observation. The J -band filter samples mainly continuum flux. Therefore, with a combination of J

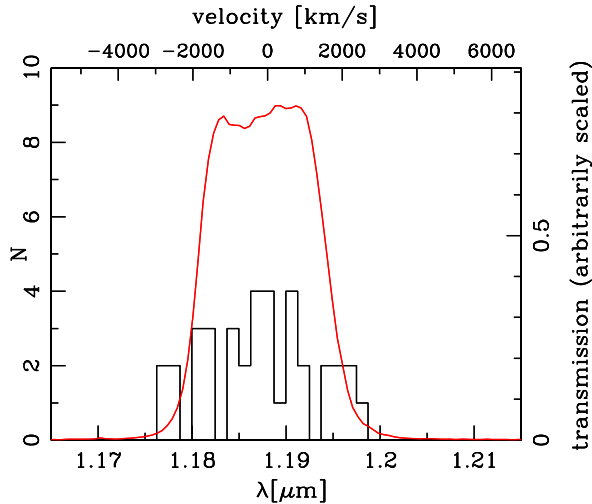


Figure 1. The transmission curve of the NB119 filter. The histogram shows the radial velocity distribution of spectroscopically confirmed members listed in Gioia et al. (1999), with respect to the velocity centre of the cluster. The wavelength of the histogram indicates the position where $H\alpha$ line of each member galaxy falls.

and NB119 filters, we can conduct an unbiased, deep $H\alpha$ imaging survey of this cluster. To neatly cover the large-scale structures discovered by Koyama et al. (2007), we set eight fields of view of MOIRCS as shown in Fig. 2. It can be seen that F1, F2, F7 and F8 have the full instrument coverage of $4' \times 7'$ (i.e. the original FoV of MOIRCS), and all the other fields, F3, F4, F5 and F6, have only a half size. Unfortunately, at the time of observation, one of the two MOIRCS chips was replaced with an engineering-grade one due to the instrumental failure. We should still stress, however, that this is the first $H\alpha$ imaging survey covering such a wide range in environment at $z \gtrsim 0.8$.

The data is reduced in a standard manner primarily using a pipeline software MCSRED (Tanaka et al. in prep). Some frames taken with NB119 show a strong fringe pattern, and we used a self-made fringe subtraction software. After matching the source positions on individual frames, we coadded to make a final image for each field, and then mosaiced all the images together. A summary of the J and the NB119 data is shown in Table 1. We match the seeing size of all the images to $0.89''$, which is the worst seeing size in the J -band. The photometric zero-points are derived using some standard stars observed on 27th May 2007. We properly scale F3–F8 data to F1 or F2 using the photometry of the same objects in the overlapping regions, although the amount of such scaling is small (<0.1 mag). We finally check that there is no significant difference in the zero-points between our FoVs using stars in the 2MASS catalogue (Jarrett et al. 2000) that fall within our observed fields. The Galactic extinction is corrected using the dust map by Schlegel, Finkbeiner, & Davis (1998). Limiting magnitudes are estimated by measuring the scatter in fluxes in randomly distributed $2''$ apertures for each FoV. Note that some overlapped regions are deeper.

2.2.2 Photometric catalogue

We first construct an object catalogue in J and NB119 with the SExtractor (Bertin & Arnouts 1996) using its two-image mode with

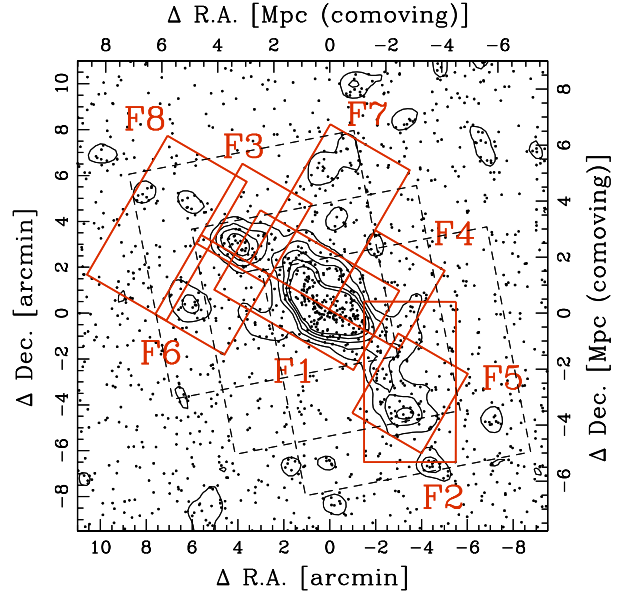


Figure 2. Our MOIRCS FoVs (F1–F8) are shown by the solid-line boxes. The three large dashed-line squares indicate the FoVs of our MIR observations with AKARI satellite ($10' \times 10'$ for each). The phot- z selected member galaxy candidates in Koyama et al. (2007) are shown by the small dots. The contours indicate 1, 2, 3, 4, 5 σ above the average local number density of the phot- z selected member candidates.

the NB119 image for source detection. We use MAG_APER ($2''$ aperture magnitude) for colours of galaxies and MAG_AUTO for total magnitudes. As shown in Table. 1, the depths of the data vary from field to field. We include objects with NB119 < 23.2 , which is $> 5\sigma$ detection in all the fields. We also require $J < 23.9$ mag ($\sim 3\sigma$ in J -band) for our sample to avoid spurious detection in NB119. After matching to the optical catalogue constructed by Koyama et al. (2007), we construct a J - and NB119-detected catalogue of the RXJ1716 cluster. Stars and objects around very bright stars are rejected through this process. The catalogue contains a full range of information of the NB119-detected galaxies, including photometries in $V R i' z' J$ and NB119 bands as well as the phot- z values from Koyama et al. (2007).

2.3 Mid-infrared(MIR) data

Koyama et al. (2008) observed this cluster at $15\mu\text{m}$ (L15 filter) with infrared camera (IRC) onboard the AKARI satellite (Onaka et al. 2007; Murakami et al. 2007). The FoVs of our MIR observations are shown with dashed-line squares in Fig. 2. It is notable that the areas of our NIR observations are mostly covered by those of MIR observations. Our $15\mu\text{m}$ filter captures the peaks of Polycyclic Aromatic Hydrocarbon (PAH: Puget & Leger 1989) emissions at rest-frame 7.7 and $8.6\mu\text{m}$ at $z \sim 0.8$, which are considered to be a good indicator of dusty star formation (e.g. Chary & Elbaz 2001). The observed $15\mu\text{m}$ flux (FLUX_AUTO value from SExtractor) is first converted to the total IR luminosity, $L(\text{IR})$, using a relation between $\nu L_{\nu, 8\mu\text{m}}$ and $L(\text{IR})$ derived from the starburst SEDs in Lagache et al. (2004) (see fig.4 of Koyama et al. 2008). Thus derived $L(\text{IR})$ is then converted to SFR using the conversion factor between SFR and $L(\text{IR})$ from Kennicutt (1998), i.e., $\text{SFR}[M_{\odot}/\text{yr}] = 4.5 \times 10^{-44} L(\text{IR})[\text{erg/s}]$.

field	Obs. date	FoV (arcmin ²)	chip	Exp. time (sec)		Limit mag. (2'', 5σ)		PSF FWHM	
				<i>J</i>	NB119	<i>J</i>	NB119	<i>J</i>	NB119
F1	2007/05/27, 2009/09/07	4' × 7'	1 and 2	3000	6000	23.5	23.3	0.6''–0.8''	0.8''
F2	2007/05/27, 2009/09/07	4' × 7'	1 and 2	2040	5100	23.5	23.3	0.6''	0.8''
F3	2008/04/19, 2008/06/30	4' × 3.5'	2	4170	4800	23.6	23.6	0.5''–0.8''	0.5''
F4	2008/06/29	4' × 3.5'	2	3840	6000	23.6	23.4	0.7''	0.6''
F5	2008/04/21, 2008/06/29	4' × 3.5'	2	3960	4500	23.4	23.3	0.6''–0.9''	0.6''
F6	2008/04/20, 2008/06/30	4' × 3.5'	2	3210	6000	23.4	23.5	0.6''–0.8''	0.6''
F7	2009/09/03, 2009/09/04	4' × 7'	1 and 2	2420	4800	23.6	23.2	0.6''–0.9''	0.8''
F8	2009/09/04, 2009/09/05	4' × 7'	1 and 2	2340	4800	23.6	23.2	0.5''	0.6''

Table 1. A summary of our near-infrared imaging data in *J* and NB119.

Note that our 5σ detection limit is 67 μJy which corresponds to SFR(IR)~15 M_⊙/yr. We adopt a 50% uncertainty in SFR(IR), which is larger than simple photometric errors, to take into account the reported uncertainty in the conversion from νL_{ν,8μm} to L(IR) (e.g. Caputi et al. 2007; Bavouzet et al. 2008). Using the MIR catalogue constructed by Koyama et al. (2008), we made a catalogue of MIR-detected galaxies within the fields covered by our MOIRCS observation. Koyama et al. (2008) constructed two types of catalogues; one for the 15 μm-resolved members (single objects) and the other for the 15 μm-unresolved members (blended objects). Likewise, we make such two types of MIR-detected catalogues in this paper as well. We derive star formation rates in IR, SFR(IR), for the 15 μm-resolved members only, since there are large uncertainty in the MIR photometries of the blended sources.

3 SELECTION OF H_α EMITTERS FROM CLUSTER MEMBERS

3.1 Selection technique

If a line emission comes into the NB119 filter, it can be identified as an object with a flux excess in NB119 compared to the *J*-band flux. Therefore the *J*–NB119 colour is a good indicator to search for emitters. However, we should take into account the fact that the NB119 filter (λ_c = 11885 Å) is located near the lower-wavelength end of *J*-band (λ_c = 12600 Å). Therefore, we cannot simply use the *J*-band magnitude as the continuum flux because the continuum flux at 1.19 μm and the *J*-band flux can be different depending on the SED slope around that wavelength regime of each galaxy. Therefore, we estimate the continuum flux level at 1.19 μm of each galaxy by linearly interpolating the magnitudes in *z'* and *J* bands. This correction substantially reduces the scatter in *J*–NB119 colours around the zero value which is expected for non-emitters in NB119 at various redshifts. We refer to such flux 'corrected' *J*-band magnitude as *J*_{corr}, and *J*_{corr}–NB119 colours of our sample are plotted against NB119 magnitudes in Fig. 3. The solid curves show ±3σ errors in *J*–NB119 colours. We define NB119 emitters as those having colour excesses of *J*_{corr}–NB119 > 0.3 and above the upper curve at the same time.

The NB119 emitters thus selected are not necessarily H_α emitters at *z* = 0.81 because other line emitters at other redshifts are also included in the NB119 emitters. For example, Hβ/[OIII] emitters at *z* = 1.4–1.5 and [OII] emitters at *z* = 2.2 are the major contaminants. We eliminate these galaxies using broad-band colours. We show in Fig. 4 a colour–colour diagram. We plot phot-*z* selected galaxies (i.e. 0.76 ≤ *z*_{phot} ≤ 0.83) as small filled circles and all the NB119 emitters as crosses. We also show the predicted

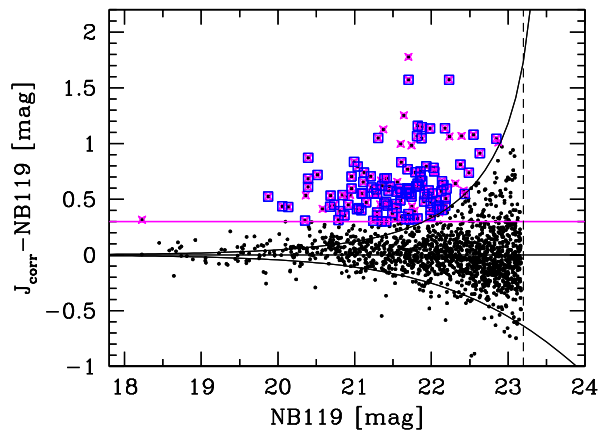


Figure 3. The narrow–broad bands colour–magnitude diagram to define our NB119 emitters. The *J*-band magnitudes are corrected for a colour-term using *z'*–*J* colours so that they correspond to the continuum fluxes at 1.19 μm. The vertical dashed-line shows 5σ limiting magnitudes in NB119 and the solid curves indicate ±3σ excess in *J*–NB119 colours. Galaxies above the horizontal solid line (*J*–NB119 = 0.3) and the upper solid curve are defined as the NB119 emitters (shown by crosses), of which the open squares show the H_α emitters at *z* = 0.81 as defined later (see text and Fig. 4).

colour tracks of model galaxies at *z* = 0.8, 1.45, 2.2, respectively, along which the contribution of bulge component is changed from 0.0 to 1.0 at each redshift (Kodama, Bell, & Bower 1999). We can see that some emitters have very different colours from the model track of *z* = 0.8 galaxies or the distribution of the phot-*z* selected galaxies. These galaxies are likely to be contaminants. We set a boundary shown by a closed box in Fig. 4, and define the H_α emitters at *z* = 0.81 as the NB119 emitters that satisfy these criteria. We may miss a few real members near the boundary, but their effect to our conclusion is negligible.

We summarize our definitions of cluster members in the following. Firstly, we select all galaxies with 0.76 ≤ *z*_{phot} ≤ 0.83 as members. This criterion recovers more than 90 % of spectroscopically confirmed members listed in Gioia et al. (1999) (see fig. 2 in Koyama et al. 2007). The same criterion is actually used in Koyama et al. (2007) and Koyama et al. (2008). The number of these phot-*z* selected members is 447. Secondly, we include all the H_α emitters at *z* = 0.81 selected above. We have 114 H_α emitters in total. Note that 32 of them have been missed out by our phot-*z* selection, although many of them have *z*_{phot} ~ 0.70–0.75, only slightly lower than our phot-*z* selection criterion. This is in-

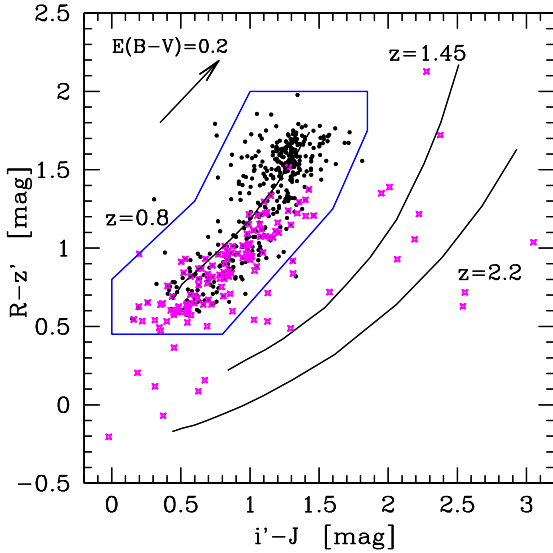


Figure 4. The colour–colour diagram to select $H\alpha$ emitters at $z = 0.81$. The phot- z selected members (filled circles) and the NB119 emitters (crosses) are plotted. Three solid curves show the colour tracks of galaxies at $z = 0.8, 1.45, 2.2$, respectively, based on the Kodama et al. (1999) model. Along the curves, the bulge fraction to the total light is changed from 0.0 to 1.0 (blue side to red side) at fixed redshift. The NB119 emitters located in the closed box are defined as $H\alpha$ emitters at $z = 0.81$. The arrow shows a reddening vector of $E(B - V) = 0.2$, calculated from the extinction law of Calzetti et al. (2000) assuming $R_V = 3.1$.

evitable since the phot- z tends to give lower redshift estimation for star-forming galaxies due to the lack of prominent features in their SED, while redshift estimation for passively evolving galaxies are relatively more accurate (e.g. Kodama, Bell, & Bower 1999). This means that the combined approach that we take in this paper, namely the phot- z selection and the narrow-band emitter survey, is quite effective to increase the completeness of true cluster members.

3.2 Local density measurements

One of the main purposes of this paper is to examine environmental dependence of $H\alpha$ -derived star formation activity at $z = 0.8$. To quantify the environment, we estimate the local density of each member galaxy using its five nearest neighbours. We already defined the local density (Σ_5 in Mpc^{-2} unit) in Koyama et al. (2008), but we recalculated it since we added 32 new members in this paper as shown in the previous section. When we calculate Σ_5 , we use all the member galaxies used in Koyama et al. (2008) (i.e. all the ~ 2700 galaxies throughout the Suprime-Cam field in the optical catalogue with $0.76 \leq z_{\text{phot}} \leq 0.83$ to the depth of $z' = 24.9$) and the 32 newly selected members. Therefore, it makes almost no change for the estimation of Σ_5 from that of Koyama et al. (2008), but the main purpose here is to define environment with Σ_5 in the same way for the newly added members.

Following the definition in Koyama et al. (2008), we classify galaxies into three environmental bins, namely, 'low-density', 'medium-density' and 'high-density' regions which correspond to $\log \Sigma_5 < 1.65$, $1.65 \leq \log \Sigma_5 < 2.15$ and $\log \Sigma_5 \geq 2.15$, respectively. The high-density region corresponds to the cluster core. The medium-density region corresponds to cluster outskirts, groups, and filaments. The low-density region corresponds to outer fields.

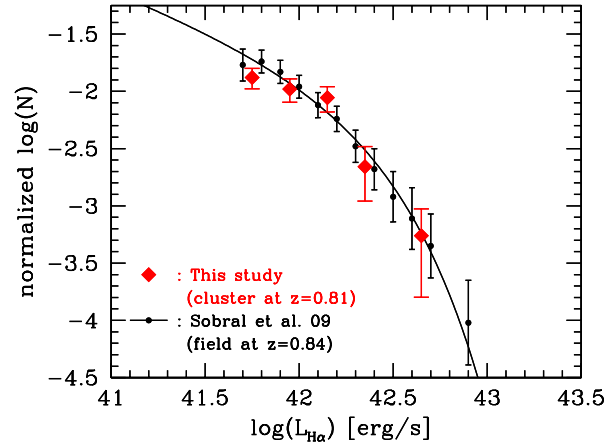


Figure 5. $H\alpha$ luminosity function of the RXJ1716 cluster (filled diamonds with purely poissonian error bars). The normalization of the cluster LF is arbitrarily scaled to compare with the field $H\alpha$ luminosity function of Sobral et al. (2009) (filled circles and their best-fitted LF as shown by the solid curve).

We note that as shown in Koyama et al. (2008) the optical colour distribution starts to change dramatically from blue to red in the medium-density environment thus defined (see also Kodama et al. 2001; Tanaka et al. 2005).

4 $H\alpha$ -DERIVED STAR-FORMATION RATE AND SPECIFIC STAR FORMATION RATE

4.1 Derivation of $\text{SFR}(H\alpha)$ and $\text{SSFR}(H\alpha)$

In this subsection, we calculate some basic physical quantities to characterize the star formation activity, such as star-formation rates (SFRs) and specific star-formation rates (SSFRs), for all the $H\alpha$ emitters. Firstly, we derive $H\alpha$ line flux, continuum flux and rest-frame equivalent width by the following equations:

$$F_{H\alpha+[NII]} = \Delta_{\text{NB}} \frac{f_{\text{NB}} - f_J}{1 - \Delta_{\text{NB}}/\Delta_J} \quad (1)$$

$$f_c = \frac{f_J - f_{\text{NB}}(\Delta_{\text{NB}}/\Delta_J)}{1 - \Delta_{\text{NB}}/\Delta_J} \quad (2)$$

$$\text{EW}_R(H\alpha + [NII]) = (1 + z)^{-1} \frac{F_{H\alpha}}{f_c} \quad (3)$$

where Δ_J and Δ_{NB} are the widths in wavelength of the J and NB119 filters, f_J is the flux density at $1.19 \mu\text{m}$ derived from the J_{corr} , and f_{NB} is the flux density for NB119. We then multiply $4\pi d_L^2$ to $F_{H\alpha+[NII]}$ to derive the luminosity $L(H\alpha + [NII])$, where d_L is the luminosity distance $5.10 \times 10^3 \text{Mpc}$ at $z = 0.81$. Finally, we compute the $H\alpha$ -based star formation rates, $\text{SFR}(H\alpha)$, using the relation of Kennicutt (1998), $\text{SFR}(H\alpha) [M_\odot/\text{yr}] = 7.9 \times 10^{-42} L_{H\alpha} [\text{erg/s}]$. We note that our selection criteria of $H\alpha$ emitters shown in Section 3.1 correspond to $\text{EW}_R(H\alpha+[NII]) \gtrsim 30\text{\AA}$ and $\text{SFR}(H\alpha) \gtrsim 1 M_\odot/\text{yr}$ before extinction correction. We correct for 30% [NII] line contribution (e.g. Tresse et al. 1999) and consider 1 mag extinction of $H\alpha$ (Kennicutt, Tamblyn, & Congdon 1994). We should note that these assumptions adopted here are somewhat uncertain and can only be applied to discuss statistical behaviours.

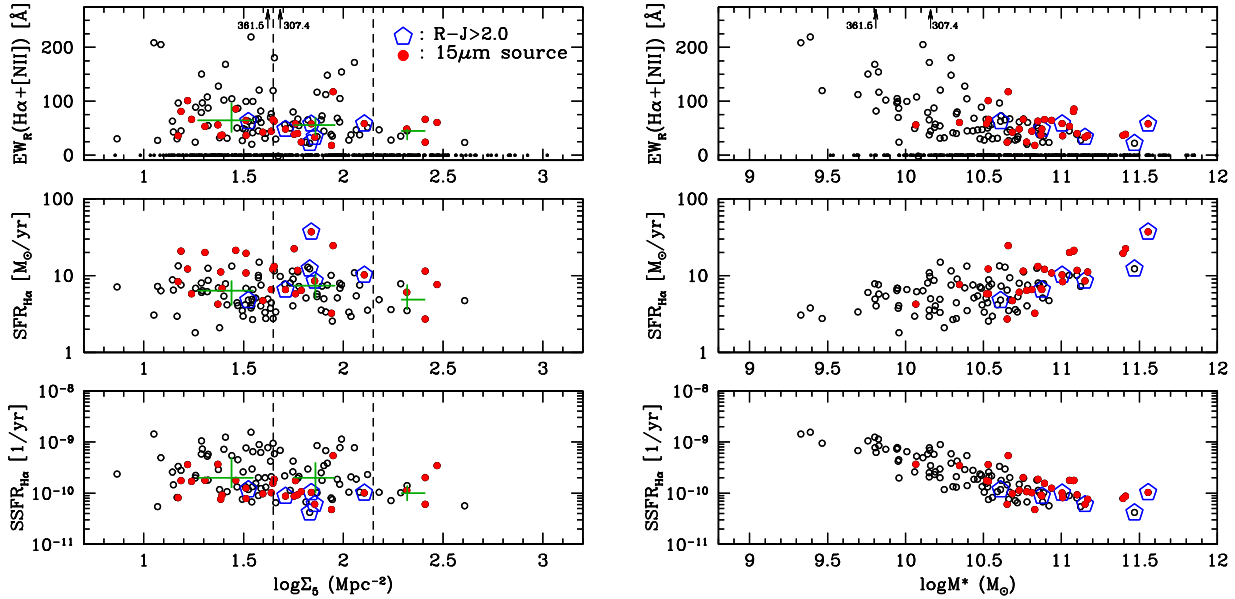


Figure 6. The physical quantities of the $H\alpha$ emitters, $EW(H\alpha+[NII])$, $SFR(H\alpha)$ and $SSFR(H\alpha)$, are plotted as a function of the local density (*left*) and stellar mass (*right*). The open circles show all the $H\alpha$ emitters, the filled circles represent the MIR galaxies and the open pentagons indicate the red $H\alpha$ emitters with $R - J > 2.0$. In SFR and SSFR, we have applied a correction for 1 mag extinction. In the top panels, the non- $H\alpha$ emitters are also plotted at $EW=0$, while only the $H\alpha$ emitters are plotted in the middle and the lower panels. The two small arrows with numbers in the top panels indicate the galaxies with high $EW(H\alpha+[NII])$ located above the top boundary. In the left panels, we show median values as crosses in each environment with error bars showing 25–75% distribution of each sample. The vertical dashed lines at $\log \Sigma_5 = 1.65$ and 2.15 in the left panels indicate the dividing lines between the low-, medium- and high-density environments as defined in Koyama et al. (2008).

In particular, the amount of extinction can be much larger for very actively star-forming galaxies (e.g. Poggianti & Wu 2000) and this will be discussed in Section 7 of this paper. We also note that we do not correct for the contamination of active galactic nuclei (AGNs) in our $H\alpha$ emitters sample. In reality, some $H\alpha$ emission lines may be originated from AGNs rather than star-forming HII regions. However, it is reported that the fraction of AGNs in distant clusters is very small (only $\sim 1\%$) from optical spectroscopic surveys (e.g. Dressler et al. 1999). The fraction of X-ray selected AGNs could be higher by a factor of ~ 5 than that of optically selected ones (e.g. Martini et al. 2002). But in any case, AGN contamination is not a major concern and has little effect on our statistical discussion on the $H\alpha$ emitters (see also Garn et al. 2009).

One of the best indicators to quantify the status of galaxy activity is the specific star-formation rate (SSFR), which is SFR divided by stellar mass of galaxies (i.e. SFR per unit stellar mass). We derive stellar mass (M_*) of galaxies in the following way. We use the relation between $M_*/L_{J(\text{obs})}$ of galaxies and $R - J$ at $z = 0.8$ for the model galaxies with different contribution of bulge component from Kodama, Bell, & Bower (1999). Note that the stellar mass in the model is re-scaled using the Salpeter IMF for consistency with the derivation of SFR. Based on the observed $R - J$ colour of each galaxy, we derive $M_*/L_{J(\text{obs})}$ which is then multiplied to the observed J -band luminosity to get M_* . SSFR is derived by dividing SFR by M_* .

4.2 $H\alpha$ luminosity function

In Fig. 5, we show the $H\alpha$ luminosity function (LF) using $H\alpha$ emitters within 2.5 Mpc from the cluster centre. We here slightly modify the selection criteria of $H\alpha$ emitters to make a fair comparison with

Sobral et al. (2009), who constructed a field $H\alpha$ LF at $z \sim 0.8$. Assuming that all $H\alpha$ emitters are associated with the cluster, we do not apply field subtraction. Our cluster LF is arbitrarily scaled to match the field $H\alpha$ LF from Sobral et al. (2009) (filled circles with their best-fitted LF). Therefore, we can only compare the shape of the cluster and field $H\alpha$ LFs. It is apparent that there is no significant difference in the shape of the $H\alpha$ LF. This is similar to the result from Kodama et al. (2004). They showed that the $H\alpha$ luminosity function shows little sensitivity to local density, using their very wide $H\alpha$ imaging around CL0024 cluster at $z = 0.39$. In the local Universe, this is also true (Balogh et al. 2004). Balogh et al. (2004) limit their sample for star-forming galaxies and showed that the strength of $H\alpha$ lines does not depend on environment. Thus, although the fraction of star-forming galaxies may change as a function of environment, star-forming activity of star-forming galaxies seems not strongly dependent on environment. Our new $H\alpha$ study for the $z = 0.81$ cluster extends this idea up to $z \sim 0.8$. As will be discussed in Section 7, there are some exceptionally active galaxies in the cluster surrounding environment. However, it would be difficult to find such excess of activity in this $H\alpha$ LF. At least, our comparison suggests that we will need much larger sample to detect the environmental difference of star-forming activity among the star-forming galaxies, if any.

4.3 Dependence on environment and stellar mass

In Fig. 6, we plot $EW_R(H\alpha+[NII])$, $SFR(H\alpha)$ and $SSFR(H\alpha)$ of $H\alpha$ emitters as a function of local density and stellar mass. It is apparent that very strong $H\alpha$ emitters with $EW \gtrsim 100 \text{ \AA}$ are seen only in the medium- and the low-density environments, and no such galaxy is found in the high-density environment (see the top-left panel of Fig.

6), although this may be due to small number statistics of the $H\alpha$ emitters in the high-density region. Other than that, we see no significant environmental trends in these quantities of the $H\alpha$ emitters. Rather, they show modest correlations with stellar mass of galaxies (right panels). Strong $H\alpha$ emitters with $EW_{\geq 100\text{\AA}}$ are found only among low mass galaxies with $\log M_* \lesssim 10.4$. More massive galaxies have higher SFRs but lower SSFRs than less massive galaxies.

We show in Fig. 7 the distribution of SSFR($H\alpha$) for each environment, dividing our $H\alpha$ emitter samples into low-mass ($\log M_*/M_{\odot} < 10.4$) and high-mass ($\log M_*/M_{\odot} > 10.4$) galaxies. We find that high-mass galaxies tend to have low SSFR ($\text{SSFR} \lesssim -9.5$) compared to low-mass galaxies in all environment. The lack of low SSFR galaxies in low-mass galaxies might be partly due to the selection effect, since the selection criteria of NB emitters is more strict for fainter galaxies as can be seen in Fig. 3. However, the lack of high mass galaxies with high SSFR should be reliable. We show the median value of SSFR($H\alpha$) in each panel as an arrow. We find that the median values do not strongly correlated with environment if we fix the stellar mass of galaxies, although the number of low-mass $H\alpha$ emitters in high-density environment is really small. We should note that this suggestion is valid only when we limit the sample to the $H\alpha$ emitters, and we should keep in mind that there are many $H\alpha$ -undetected galaxies in particular in higher-density environments (see Section 5).

We plot the MIR-detected galaxies as filled symbols in Fig. 6. We can notice that the MIR-detected galaxies tend to have low $EW(H\alpha + [NII])$ and low SSFR($H\alpha$) in spite of their high star formation rates in MIR ($\text{SFR}(\text{IR}) \geq 15 M_{\odot}/\text{yr}$). One may claim that MIR-detected galaxies tend to be biased to more massive galaxies with larger SFR. However, interestingly, there is no significant difference in SFR($H\alpha$) between MIR-detected and MIR-undetected galaxies (see middle-right panel in Fig. 6). There is a trend that massive $H\alpha$ emitters tend to be detected in MIR, indicating that they tend to be more dusty, hence their SFRs (and SSFRs) are likely to be underestimated even with $H\alpha$. This suggests that we need not only $H\alpha$ information but also MIR information to fully understand the star formation history of massive galaxies in the distant Universe. In the remaining of this paper, taking the great advantage of wide-field coverage of our $H\alpha$ and MIR data, we attempt to show how large amount of star-formation is obscured and hidden in the previous optical surveys and how the obscuration is related to environment at $z \sim 0.8$ for the first time.

5 MAPPING OUT STAR-FORMATION ACTIVITY IN AND AROUND THE CLUSTER

5.1 Spatial distribution

We show in the left panel of Fig. 8 the spatial distribution of cluster member galaxies (small open circles), blue $H\alpha$ emitters with $R - J < 2.0$ (open squares) and red $H\alpha$ emitters with $R - J > 2.0$ (open pentagons). We only plot the galaxies in the area observed by the NB filter. We can see that $H\alpha$ emitters well trace the filamentary large-scale structures. This is a strong evidence for that most of the small groups identified by phot- z are physically associated with the cluster and not just a concentration of fore-/background galaxies. Note that we may be missing some $H\alpha$ emitters especially in the outskirts of the clusters, where relative velocities of galaxies with respect to the cluster core would be larger, although the width of the NB119 filter neatly covers the radial velocity range of \pm

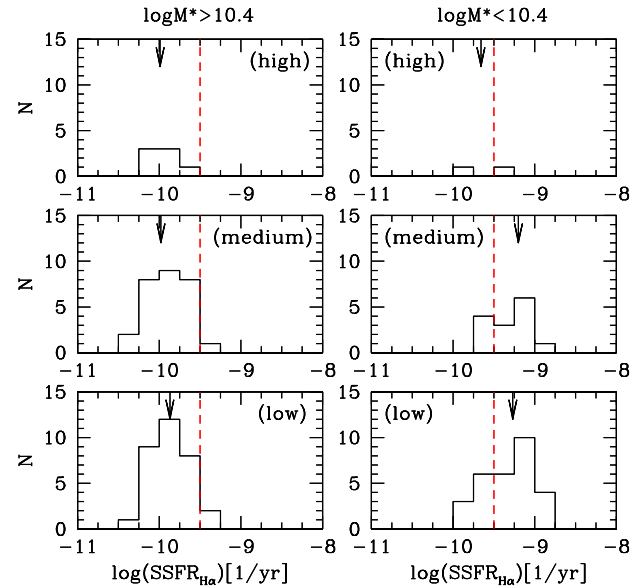


Figure 7. The distributions of SSFR for high-mass ($\log M_*/M_{\odot} > 10.4$) and low-mass ($\log M_*/M_{\odot} < 10.4$) galaxies in each environmental bin for all the $H\alpha$ emitters. The arrows indicate the median value of SSFR in each panel. The vertical dashed lines at $\text{SSFR} = -9.5$ show the dividing line between the high and low SSFR galaxies for an eye-guide.

$\sim 1500 \text{ km s}^{-1}$ (see Fig. 1). A $5' \times 5'$ close-up view is shown in the right panel of Fig. 8. We also plot the position of MIR-detected galaxies (including resolved and unresolved objects) as filled circles. It can be easily noticed that the distribution of $H\alpha$ emitters is quite similar to that of MIR-detected galaxies. We reported the avoidance of MIR-detected galaxies in the cluster central region in Koyama et al. (2008), and this study strengthens the conclusion that the star-forming activity is very low in the cluster core of this cluster.

On the other hand, it is interesting to note that the $H\alpha$ emitters and MIR-detected galaxies do not always directly overlap each other. Since our $H\alpha$ survey can go deeper in terms of SFR ($\sim 1 M_{\odot}/\text{yr}$ without extinction correction) compared to MIR observation ($\sim 15 M_{\odot}/\text{yr}$), it is natural to expect that some moderately (or weakly) star-forming galaxies are detected only in $H\alpha$. In fact, we can see many such galaxies in Fig. 8. However, there are also some galaxies which are detected in MIR but not in $H\alpha$. These type of galaxies are difficult to interpret. It may be possible that these galaxies are very dusty and a large amount of UV/optical light is hidden by dust, so that we cannot detect their $H\alpha$ emission lines. It is also possible that some MIR galaxies are located outside of the redshift range of the $H\alpha$ emitters that is covered by the NB119 filter. Some of them can still be members (see Fig. 1), but some could be non-member contaminants due to the limitation of phot- z based membership determination of the MIR galaxies. Spectroscopic confirmation of their membership is needed to discuss this interesting population further.

5.2 $H\alpha$ fraction

As shown in the previous section, $H\alpha$ emitters avoid cluster central region and/or high-density region. We quantify it by calculating the fraction of $H\alpha$ emitter as functions of local density and cluster

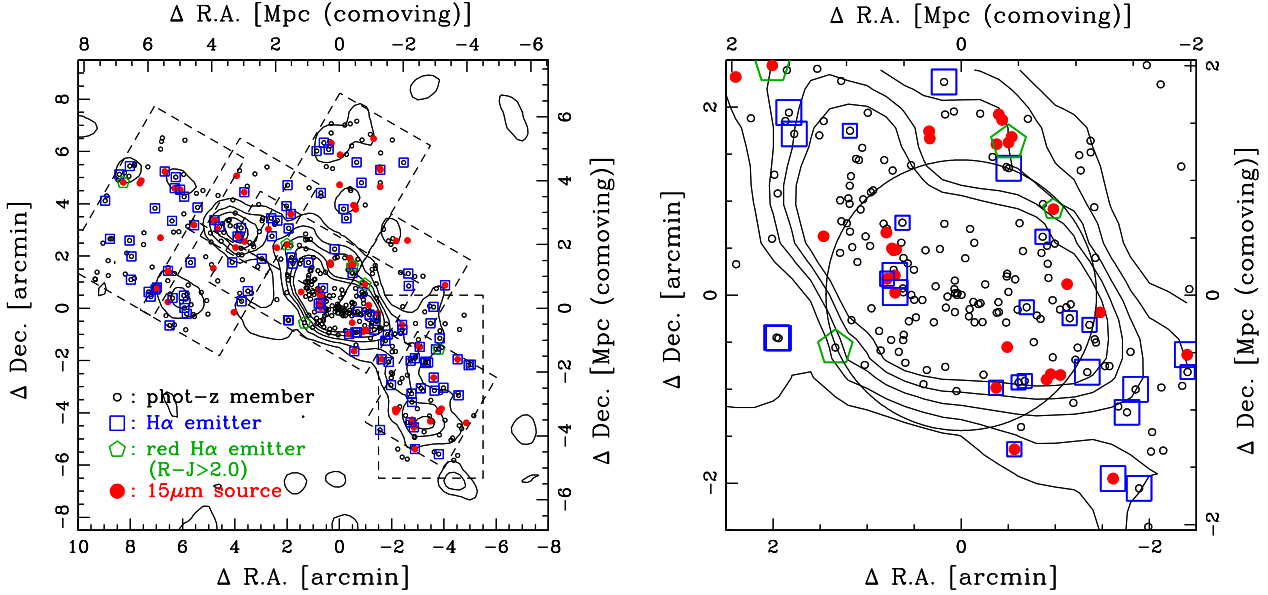


Figure 8. (*left*): The 2-D distributions of all the members (open circles), the MIR-detected galaxies (filled circles), the blue $H\alpha$ emitters with $R - J < 2.0$ (open squares), and the red $H\alpha$ emitters with $R - J > 2.0$ (open pentagons). The dashed-line boxes indicate our MOIRCS FoVs. We plot the member galaxies detected in our MOIRCS FoVs only. The contours are the same as in Fig. 2. (*right*): A close-up view of the cluster central region. The meanings of the symbols are the same as in the left panel, except that the large and the small open symbols indicate the strong ($EW > 50\text{\AA}$) and weak ($EW < 50\text{\AA}$) $H\alpha$ emitters, respectively. The solid-line circle shows the radius of $0.5 \times R_{200}$ from the cluster centre (see Section 8).

centric radius (Fig. 9). We use galaxies with $NB119 < 22.0$ where the selection of $H\alpha$ emitters is complete down to $J - NB119 = 0.3$ (see Fig. 3). It can be seen that the $H\alpha$ fraction is strongly dependent on local density and cluster centric radius, in the sense that the fraction is lower in the higher-density environment. Thus, we conclude that there is little star-formation activity in the core of the RXJ1716 cluster. Such global trend that the fraction of $H\alpha$ emitters decreases towards higher density regions (Fig. 9) is largely due to the fact that the fraction of passive galaxies increases towards higher density regions. In fact, if we limit the sample only to blue galaxies with $R - J < 2.0$, the fraction of $H\alpha$ emitters does no longer strongly correlate with local density or cluster centric radius, and is almost constant at $\sim 60\%$. This is consistent with the results obtained in Section 4.2 and 4.3 that the observed $H\alpha$ line strength in star-forming galaxies does not strongly correlate with environment.

Finn et al. (2005) conducted similar $H\alpha$ emitter survey for the central part of three $z \sim 0.7$ clusters. They showed that two of the three clusters have few $H\alpha$ emitters in the central region. However, they found many $H\alpha$ emitters in the core region of the other cluster. Hayashi et al. (2009) show that there are many [OII] emitters even in the cluster core at $z = 1.46$, and that the fraction of [OII] emitters is still high in the core within $R_c < 0.25$ Mpc from the cluster centre. For the RXJ1716 cluster, we find no $H\alpha$ emitters at $R_c < 0.25$ Mpc as shown in the right-panel of Fig. 9, although there are 31 member galaxies in $R_c < 0.25$ Mpc without significant detection in $H\alpha$. Therefore, for the RXJ1716 cluster, the termination of star-forming activity in the cluster core has been completed before $z = 0.8$. These facts suggest that the epoch of the termination of star-forming activity in the cluster core may differ from cluster to cluster, probably depending on the cluster mass and/or maturity of clusters. We need a much larger sample of distant clusters to draw a general picture of formation and evolution of the cluster cores.

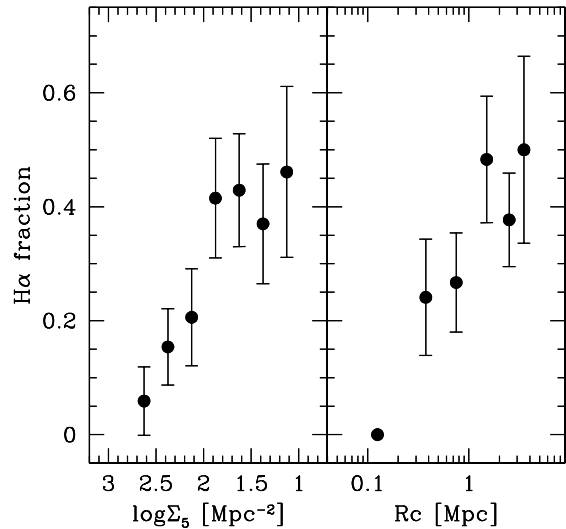


Figure 9. The fraction of the $H\alpha$ emitters as a function of local density (*left*) and as a function of cluster-centric distance (*right*). The error-bars show Poisson errors.

6 PROPERTIES OF $H\alpha$ EMITTERS AND MIR GALAXIES

6.1 Colour-magnitude diagram

In Fig. 10, we show $(R - J)$ v.s. J colour-magnitude diagram using all the member galaxies. $H\alpha$ emitters are marked with open squares again. The small and large sizes of squares indicate $EW(H\alpha + [NII]) < 50\text{\AA}$ and $EW(H\alpha + [NII]) > 50\text{\AA}$, respectively. We clearly notice that $H\alpha$ emitters are mainly blue galaxies and that

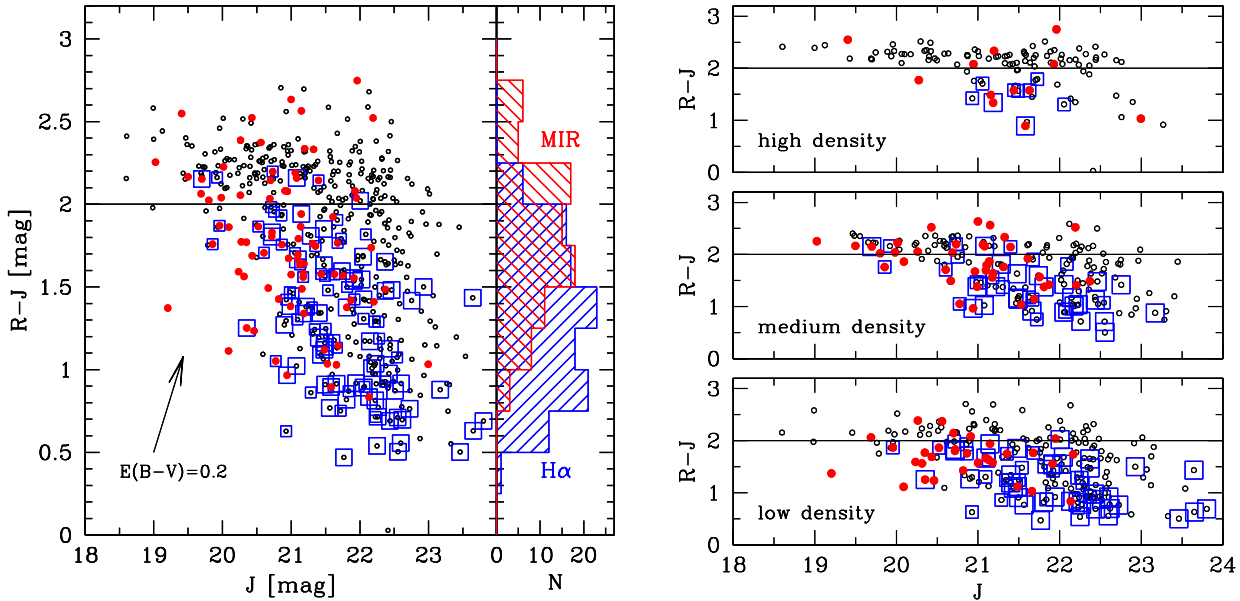


Figure 10. (*left*): The colour–magnitude diagram for all the observed fields. The open circles show all the member galaxies. The small and large open squares indicate the weak ($EW < 50\text{\AA}$) and strong ($EW > 50\text{\AA}$) $H\alpha$ emitters, respectively. The filled circles indicate the MIR galaxies. The histograms show the colour distributions of the $H\alpha$ emitters and the MIR galaxies as indicated. The arrow shows a reddening vector that corresponds to $E(B - V) = 0.2$. (*right*): The same plot for each environment (low-, medium- and high-density regions). The meanings of the symbols are the same as in the left panel.

bluer galaxies tend to have stronger $H\alpha$ emission in an average sense. There are also some $H\alpha$ emitters on the red sequence. These populations are very rare, but interestingly, we find that such $H\alpha$ emitters with red colours are preferentially found in the cluster outskirts (see below). On the other hand, MIR galaxies (shown as filled circles in Fig. 10) are more commonly seen on the red sequence. This is clearly seen in the histograms shown in Fig. 10. The $H\alpha$ emitters are bluer and the MIR galaxies are redder. This may be because the MIR galaxies are dusty and reddened in spite of their strong star formation (see also Koyama et al. 2008).

We also make the same plot for each environment (i.e. for low-, medium- and high-density regions) in the right-panels of Fig. 10. Interestingly, the red sequence appears quite differently with environment. Most of the red galaxies in the high-density and low-density environment show little on-going star-forming activity. In contrast, a large number of red galaxies in the medium-density environment (i.e. in the cluster outskirts, groups and filaments) are detected in $H\alpha$ and/or MIR. We detect 6 red $H\alpha$ emitters in total, of which 5 are found in the medium-density environment. We have already reported in Koyama et al. (2008) a high fraction of MIR-detected dusty red galaxies in the medium-density environment. The above result on the $H\alpha$ emitters supports this idea. Saintonge, Tran, & Holden (2008) showed that the number of MIR galaxies on the red sequence increases towards distant clusters up to $z \sim 0.8$. Our current result suggests that the MIR view of the red sequence is also dependent on environment at $z \sim 0.8$.

6.2 Colour–colour plot

We show in Fig. 11 the colour–colour diagrams ($R - z'$ v.s. $z' - J$). Using the three bands that neatly straddle the rest-frame 4000\AA break, we can effectively distinguish dusty red galaxies from passively evolving red galaxies. This method is similar to the one

used to distinguish between dusty and passive galaxies for the sample of the extremely red objects (EROs) at $z \sim 1.5$ (e.g. Pozzetti & Mannucci 2000).

In the top-left panel of Fig. 11, we notice that the star-forming galaxies (i.e. $H\alpha$ emitters and MIR galaxies) are distributed in an elongated region along the direction of the reddening vector (shown by the arrow). In contrast, non-star-forming galaxies (small dots) are concentrated at around $R - z' \sim 1.6$ and $z' - J \sim 0.6$. Thus, we can separate between passive galaxies and star-forming galaxies on this diagram. Many of the MIR galaxies are red in a single colour in Fig. 10, but with an appropriate colour combination here, the passive galaxies and the dusty star-forming galaxies occupy different areas on the diagram and can be well separated.

In Fig. 11, we also make the same plot for each environment. As is also seen in Fig. 10, $H\alpha$ emitters are blue and MIR galaxies are redder. Most of the red star-forming galaxies are detected only in MIR and even not in $H\alpha$. Such red MIR galaxies are frequently seen in the medium-density environment. We also find that very blue galaxies are detected only in $H\alpha$ but not in MIR (as seen in Fig. 10). This may be because bluer galaxies tend to be lower-mass galaxies (see Fig. 10) and to have lower SFR (see Fig. 6), so that we could not detect many of these low-mass star-forming galaxies by our MIR observation due to the MIR flux limit.

6.3 Colour–density plot

As we showed in the previous sections, the nature of star-forming activity of galaxies is related to environment (i.e. galaxy density). In Fig. 12, we plot $R - J$ colours as a function of the local density. This plot would be a good summary of our important findings.

Firstly, colours of galaxies start to change at the medium-density environment. Clearly, the number of blue galaxies (with $R - J < 2.0$) decreases in high-density environment ($\log \Sigma_5 >$

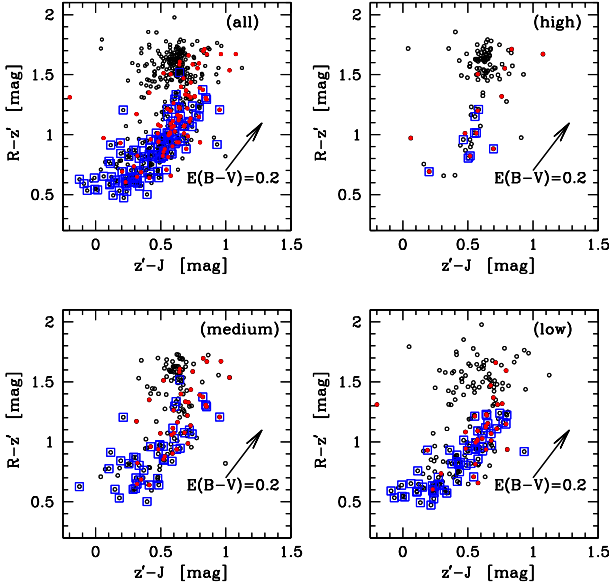


Figure 11. The colour–colour diagram ($R - z'$ vs. $z' - J$) for all the observed fields (top-left panel), the high-density region (top-right), the medium-density region (bottom-left), and the low-density region (bottom-right), respectively. The small open circles represent all the member galaxies. The open squares and the filled circles indicate the $H\alpha$ emitters and the MIR galaxies, respectively. The arrows indicate reddening vectors corresponding to $E(B - V) = 0.2$.

2.15). This is quantified by calculating the fraction of red galaxies (with $R - J > 2.0$) as a function of the local density (the solid-line locus in Fig. 12). This result is consistent with our previous finding in Koyama et al. (2008), who made a similar plot and examined $R - z'$ colour using all optical sources. We confirm the trend that galaxy properties are changed not only in cluster environment but also in relatively low-density groups and filaments.

Secondly, we notice that most of the $H\alpha$ emitters are blue, but there exist some red emitters with $R - J > 2.0$. These galaxies are candidates of dusty star-forming galaxies, and interestingly, these galaxies are preferentially found in the medium-density environment. In fact, we have 6 such red $H\alpha$ emitters in total and 5 out of 6 are in the medium-density environment. Also, 4 out of 6 such emitters are detected in MIR. This indicates that these red $H\alpha$ emitters are not just ceasing their star-formation. Rather, it seems that they have very strong star-formation but are heavily attenuated by dust.

Thirdly, the MIR galaxies are generally redder than the $H\alpha$ emitters, and some of them are located on the red sequence. Such optically red MIR galaxies are also preferentially found in the medium-density region (i.e. transition environment) and some of them are not detected in $H\alpha$.

It turns out that a fraction of the red galaxies in the cluster surrounding regions are dusty star-forming galaxies, which would have been difficult to be distinguished from passively evolving red galaxies with optical colour information alone. In contrast, most of the red galaxies in the high-density environment are passive galaxies with little on-going star-forming activity. This may indicate that we are witnessing the transition phase of galaxies in the cluster outskirts when/where some galaxies experience an active, but dusty

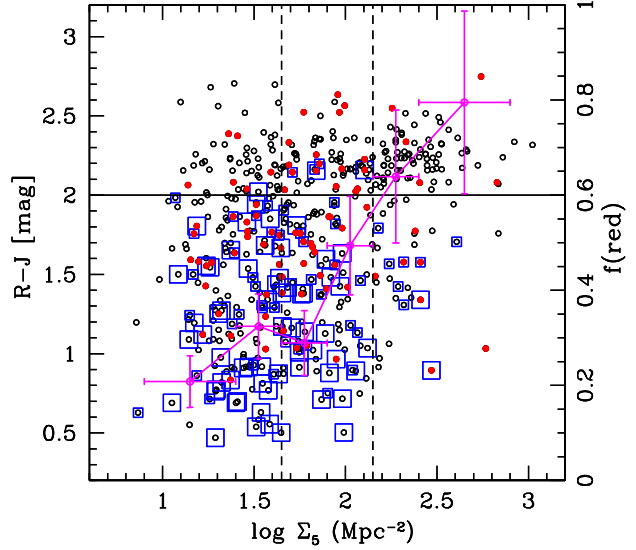


Figure 12. The colour–density plot for all the member galaxies (open circles). The small and large open squares indicate the weak ($EW < 50\text{\AA}$) and strong ($EW > 50\text{\AA}$) $H\alpha$ emitters, respectively. The filled circles show the MIR galaxies. The dashed lines at $\log \Sigma_5 = 1.65$ and 2.15 indicate the dividing lines between the low-, medium- and high-density regions as defined in Koyama et al. (2008). The solid-line shows the locus of the fraction of red galaxies calculated using our NIR-detected members. The vertical and horizontal error-bars indicate Poisson errors and the size of the environmental bins used for $f(\text{red})$, respectively.

star-forming phase before being truncated. More detailed discussion will follow in the next section.

7 HIDDEN ACTIVITY IN DISTANT CLUSTERS

7.1 Comparison between $H\alpha$ and MIR activity

As suggested in the previous section, a significant fraction of star formation activity is likely to be hidden in the optical data even in the $H\alpha$ data, in particular in the surrounding regions of high- z clusters. To quantify the amount of hidden star formation, we calculate the ratio of $\text{SFR}(\text{IR})$ to $\text{SFR}(\text{H}\alpha)$ for our MIR-detected galaxies down to 3.5σ in detection ($\sim 10M_{\odot}/\text{yr}$). Here, we measure $\text{SFR}(\text{H}\alpha)$ for the members that satisfy $J - \text{NB119} > 0.15$ instead of $J - \text{NB119} > 0.3$ that we used in Section 3.1, so that we can reach to fainter MIR-detected galaxies. In Fig. 13, we plot the ratios, $\text{SFR}(\text{IR})/\text{SFR}(\text{H}\alpha)$, as a function of $\text{SFR}(\text{IR})$. Here, we do not apply for any extinction correction in deriving $\text{SFR}(\text{H}\alpha)$. We see a weak trend that galaxies with higher $\text{SFR}(\text{IR})$ tend to have higher $\text{SFR}(\text{IR})/\text{SFR}(\text{H}\alpha)$ ratios. This is consistent with previous studies which show that the dusty component of star formation rate becomes higher as total star formation rate goes up (e.g. Geach et al. 2006; Dopita et al. 2002; Garn et al. 2009). We can also notice that red MIR galaxies (shown as filled symbols in Fig. 13) tend to have higher $\text{SFR}(\text{IR})/\text{SFR}(\text{H}\alpha)$ ratios. This is reasonable because their red colours can be the results of heavy dust attenuation.

The absolute values of $\text{SFR}(\text{IR})/\text{SFR}(\text{H}\alpha)$ span widely from ~ 2 to ~ 40 , depending on their $\text{SFR}(\text{IR})$. For moderately star-forming galaxies (i.e. $\text{SFR}(\text{IR}) \sim 10M_{\odot}/\text{yr}$), the extinction of $H\alpha$ strength seems to be ~ 1 mag, in excellent

agreement with the study of local star-forming galaxies (e.g. Kennicutt, Tamblyn, & Congdon 1994). However, for actively star-forming galaxies (i.e. $\text{SFR}(\text{IR}) \gtrsim 20 M_{\odot}/\text{yr}$), the magnitude of obscuration is significantly large and $A_{H\alpha}$ can exceed ~ 3 mag in the extreme cases, even though $H\alpha$ line is considered as one of the most reliable SFR indicators. There have been some pieces of evidence for such large amount of obscuration in actively star-forming IR galaxies. For example, Poggianti & Wu (2000) presented spectral natures of IR galaxies at intermediate redshifts, and showed that these galaxies tend to be classified as 'e(a)', which show emission lines as a sign of moderate star formation activity and strong balmer absorption at the same time. In fact, they showed $\text{SFR}(\text{IR})/\text{SFR}(\text{H}\alpha) \sim 10\text{--}70$, and this is in good agreement with our values. In cluster environments, Smail et al. (1999) conducted deep radio observations in the CL0939 cluster at $z = 0.41$. They detected radio continuum light at 1.4GHz, as a sign of on-going star formation activity, from the galaxies which have been classified as post-starburst galaxies by optical spectra based on the presence of strong balmer absorption lines and the absence of emission lines. Recently, Dressler et al. (2009) conducted MIR observation of the A851 cluster at $z = 0.41$. They detected MIR emission not only from the majority of e(a) galaxies but also interestingly from $\sim 30\%$ of k(a) galaxies (i.e. post-starburst galaxies with no emission lines). These results all indicate that the optical signs of star-forming activity tend to be weak especially for galaxies with strong star formation that are well traced by MIR observations, and thus can be sometimes misleading.

In fact, our MIR galaxies in RXJ1716 do not show strong $H\alpha$ emissions. As shown in Fig. 6, we find that $\text{EW}(H\alpha + [\text{NII}])$ and $\text{SSFR}(H\alpha)$ of the MIR-detected galaxies tend to be lower than those of the MIR-undetected $H\alpha$ emitters. Also, the MIR galaxies are sometimes 'not' detected as $H\alpha$ emitters. Unfortunately, we do not have any spectroscopic information for these galaxies yet. It is possible that these galaxies are even more heavily obscured objects, but in the current situation, we cannot exclude the possibility that these galaxies are located at slightly lower or higher redshifts and their $H\alpha$ lines do not fall within the NB119 filter. Therefore, we limit the sample to the galaxies with $H\alpha$ detection in this paper because these galaxies are reliable members. We will present spectroscopic data of this cluster to reveal the nature of MIR galaxies undetected in $H\alpha$ in a forth-coming paper.

7.2 Environmental dependence of the hidden activity ?

Taking the unique advantage of the wide-field coverages of our both $H\alpha$ and MIR imaging surveys presented in this paper, we attempt to examine the environmental dependence of 'hidden' star-formation around a $z \sim 0.8$ cluster for the first time. In Fig. 13, we use different symbols depending on their environment (squares for low-density, triangles for medium-density and circles for high-density). Interestingly most of the 'heavily attenuated' galaxies (e.g. $\text{SFR}(\text{IR})/\text{SFR}(\text{H}\alpha) \gtrsim 15$) are located in the medium-density regions. Although the number of MIR galaxies is not large, there is a hint that very dusty galaxies most frequently appear in groups/filaments where galaxy properties are dramatically changed (see Section 6.3). Note that some of those galaxies in the outskirts may have large relative velocities with respect to the cluster core and their $H\alpha$ lines may fall on the wings of the transmission curve of the NB119 filter, and therefore their $\text{SFR}(\text{H}\alpha)$ may be underestimated. Their red colours, however, indicate that they are indeed dusty objects. Also, it can be seen that bright MIR galaxies (e.g. $\text{SFR}(\text{IR}) \gtrsim 40 M_{\odot}/\text{yr}$) are found only in the medium-

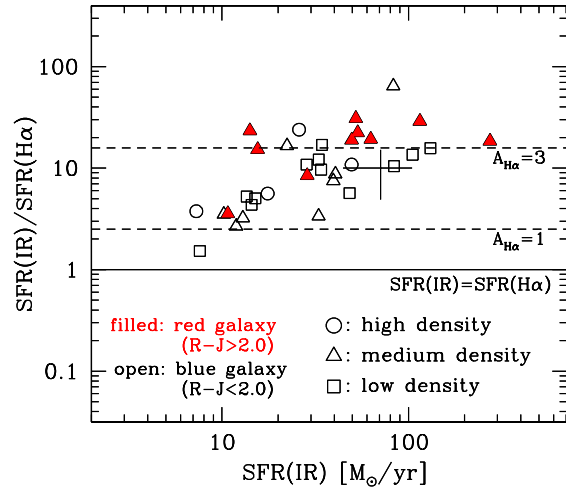


Figure 13. The ratios of $\text{SFR}(\text{IR})$ to $\text{SFR}(\text{H}\alpha)$ plotted against $\text{SFR}(\text{IR})$. We plot only the $H\alpha$ emitters with $J_{\text{corr}} - \text{NB119} > 0.15$ that are detected as single objects at MIR with detection significance of $> 3.5\sigma$. The squares, triangles, and the circles indicate the galaxies in the low-, medium-, and high-density environments, respectively. The filled symbols show the red galaxies with $R - J > 2.0$. A representative error bar is shown as the cross. The uncertainty in $\text{SFR}(\text{H}\alpha)$ corresponds to a 1σ error in the aperture photometry, while we adopt a 50% error in $\text{SFR}(\text{IR})$ to take into account the large uncertainty in the conversion from $\nu L_{\nu, 8\mu\text{m}}$ to $L(\text{IR})$ (see text).

and low-density environments, but no such galaxies are found in the high-density region. These results are consistent with our findings in Section 6 where we find many dusty red galaxies in the medium-density regions. Such enhanced dusty star-formation in the intermediate-density environment has also been reported for lower- z samples in the literature (e.g. Wolf, Gray, & Meisenheimer 2005; Fadda et al. 2008; Gallazzi et al. 2009; Tran et al. 2009). Our current results show a similar trend up to $z \sim 0.8$. Our unique wide-field $H\alpha$ and MIR surveys in and around the RXJ1716 cluster demonstrate the necessity of wide-field IR observations covering the transition environment in the cluster suburbs in order to reveal the key processes to shape the environmental dependence of galaxy evolution and its link to IR activity of galaxies.

8 GLOBAL EVOLUTION OF STAR-FORMATION ACTIVITY IN CLUSTERS

8.1 $H\alpha$ view of the cluster evolution

In this final section, we discuss the global evolution of star formation activity in clusters together with the previous $H\alpha$ cluster studies in the literature. Finn et al. (2005) sketched the evolution of $H\alpha$ -derived total SF in clusters ($\Sigma\text{SFR}_{H\alpha}$) and that divided by cluster mass ($\Sigma\text{SFR}_{H\alpha}/M_{cl}$) as a function of cluster redshift (see also Kodama et al. 2004). We now estimate these quantities ($\Sigma\text{SFR}_{H\alpha}$ and $\Sigma\text{SFR}_{H\alpha}/M_{cl}$) for the RXJ1716 cluster. Finn et al. (2005) used all the cluster member galaxies within $0.5 \times R_{200}$ for each cluster to derive $\Sigma\text{SFR}_{H\alpha}$ and divide $\Sigma\text{SFR}_{H\alpha}$ by M_{200} for each cluster to derive $\Sigma\text{SFR}_{H\alpha}/M_{cl}$. The radius and mass (R_{200} and M_{200}) of each cluster are defined by the following equations:

$$R_{200} = 2.47 \frac{\sigma}{1000 \text{ km/s}} \frac{1}{\sqrt{\Omega_{\Lambda} + \Omega_0(1+z)^3}} \text{ Mpc} \quad (4)$$

$$M_{cl} = 1.71 \times 10^{15} \left(\frac{\sigma}{1000 \text{ km/s}} \right)^3 \frac{1}{\sqrt{\Omega_{\Lambda} + \Omega_0(1+z)^3}} M_{\odot} \quad (5)$$

where σ is the velocity dispersion of the cluster. However, for an unrelaxed cluster such as this RXJ1716 cluster, the velocity dispersion tends to be over-estimated due to the presence of kinematical substructures. In fact, the velocity dispersion of the RXJ1716 cluster is estimated to be $\sim 1500 \text{ km/s}$ in Gioia et al. (1999), which is much larger than that estimated from its X-ray temperature ($\sim 600 \text{ km/s}$) as they noted. Based on the new X-ray measurement in Ettori et al. (2004), we re-estimate the velocity dispersion to be $\sigma = 837 \text{ km/s}$. Based on this value, we derive $R_{200} = 1.3 \text{ Mpc}$ and $M_{200} = 6.5 \times 10^{14} M_{\odot}$ for the RXJ1716 cluster. We then integrate SFR($H\alpha$) of the member galaxies detected at more than 3σ level in $H\alpha$ within $0.5 \times R_{200}$, and correct for incompleteness due to the wings of the filter response function by multiplying a factor ~ 1.4 to derive $\Sigma \text{SFR}_{H\alpha}$. We show our measurements, $\Sigma \text{SFR}_{H\alpha} = 210 \pm 42 M_{\odot}/\text{yr}$, in Fig. 14 with those of other clusters in Finn et al. (2005) (i.e. originally from Balogh et al. 2002 for A1689, Balogh & Morris 2000 for A2390, Couch et al. 2001 for AC114, Kodama et al. 2004 for CL0024, Finn et al. 2005 for CL1040, CL1054-12 and CL1216, and Finn, Zaritsky, & McCarthy 2004 for CLJ0023+0423B). As can be seen in Fig. 14, we find no significant evolution in $\Sigma \text{SFR}_{H\alpha}$ with redshift (lower panel), while $\Sigma \text{SFR}_{H\alpha}/M_{cl}$ seems to increase towards higher redshift clusters (upper panel). Although the scatter at a given redshift is very large, $\Sigma \text{SFR}_{H\alpha}/M_{cl}$ approximately scales with $(1+z)^6$ as shown by a solid curve in the top panel of Fig. 14.

It is possible that the scatter among clusters at a similar redshift is due to the difference in cluster mass. As shown in Fig. 15, $\Sigma \text{SFR}_{H\alpha}/M_{cl}$ is well correlated with cluster mass, in consistent with Finn et al. (2005) (see also Poggianti et al. 2006 and Homeier et al. 2005). It may indicate that the cluster mass is also an important factor to determine cluster properties. We should note, however, that the determination of cluster mass is highly uncertain and this could be the biggest source of uncertainty in drawing any general picture of cluster evolution. In fact, if we take $\sigma \sim 1500 \text{ km/s}$ as derived from the optical spectroscopy in Gioia et al. (1999), $\Sigma \text{SFR}_{H\alpha}$ increases by a factor of ~ 2 and $\Sigma \text{SFR}_{H\alpha}/M_{cl}$ decreases by a factor of ~ 3 . We would need a much larger sample of clusters to obtain more secure trend.

8.2 MIR view of the cluster evolution

In the previous sub-section, we have examined the evolution of star-forming activity in clusters based on $H\alpha$ intensity assuming a constant 1-magnitude extinction correction for all the emitters. This assumption is valid for moderately or weakly star-forming galaxies, but much larger extinction correction would be needed for very actively star-forming galaxies (see Fig. 13). In order to take into account the hidden star-formation as much as possible, we now use SFR(IR) for the MIR-detected galaxies while we stick to use SFR($H\alpha$) with 1-mag correction for the MIR-undetected galaxies, and sum up all the SFR within $0.5 \times R_{200}$ from the cluster centre. In this calculation, we included the blended MIR sources as well, and used the combined MIR flux of such sources. These all sum up to the total SFR($H\alpha$ +MIR) of $\sim 620 \pm 250 M_{\odot}/\text{yr}$, which is more than factor 2 larger than the integrated SFR($H\alpha$) even after applying for the constant 1-mag extinction correction. Note that we adopt a 50% uncertainty in ΣSFR_{IR} , which is the same amount as what we assumed in SFR(IR) for individual galaxies (Section 2.3).

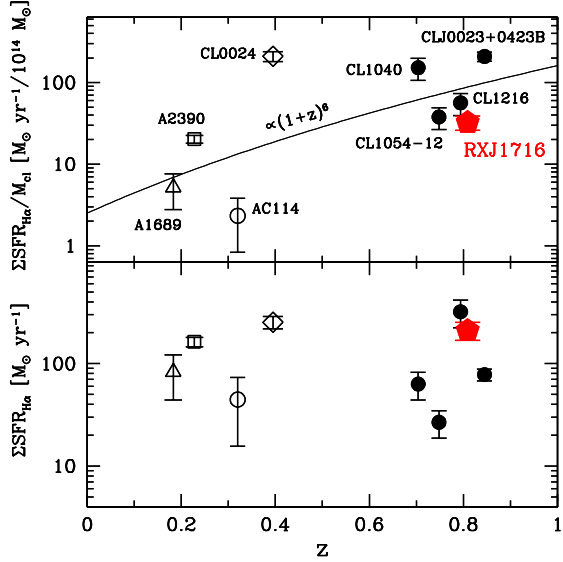


Figure 14. (*bottom*): The integrated total SFR($H\alpha$) within $0.5 \times R_{200}$ as a function of redshift. (*top*): The integrated total SFR($H\alpha$) normalized by the cluster mass M_{200} as a function of redshift.

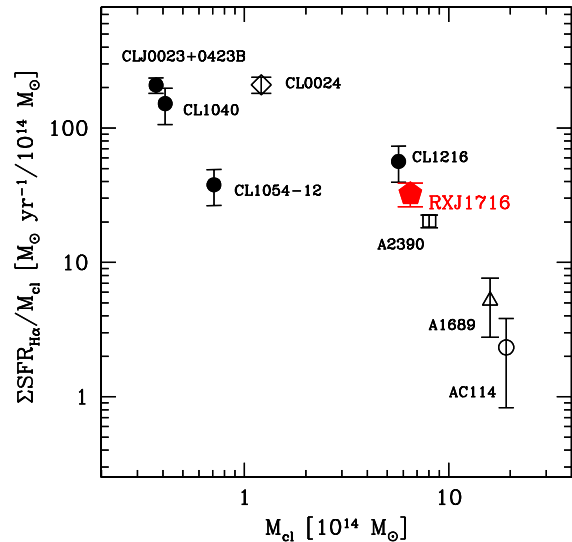


Figure 15. The integrated total SFR($H\alpha$) normalized by the cluster mass as a function of cluster mass, M_{200} . The symbols are the same as in Fig. 14. Open and filled symbols indicate the low- z samples ($z \lesssim 0.4$) and the high- z samples ($z \gtrsim 0.6$), respectively.

This may be an overestimation for an integrated quantity ΣSFR_{IR} , but we take it as a conservative error.

We suggest that non-negligible fraction of star-forming activity in clusters is hidden by dust and thus strongly supports the importance of IR study of distant clusters and/or accurate extinction correction to obtain true SFRs and to quantify the evolution of star-forming activity in clusters. Although the number of known clusters studied so far in MIR is very small, some authors have

attempted to sketch the global evolution of star formation activity in clusters based on the MIR-derived SFRs (Geach et al. 2006; Bai et al. 2007, 2009; Haines et al. 2009a; Krick et al. 2009). We here follow the scheme in Bai et al. (2007), who measured integrated cluster SFR(IR) within $0.5 \times R_{200}$ from the cluster centre. Their flux limit in IR corresponds to $\sim 10 M_{\odot}/\text{yr}$ at $z \sim 0.8$, but they integrated SFR down to $\sim 2 M_{\odot}/\text{yr}$ by extrapolating their IR luminosity function to that depth. We can go down to the similar depth by combining the MIR- and H α -derived SFRs within $0.5 \times R_{200}$ of the RXJ1716 cluster. In Fig. 16, we show the total SFR(H α +MIR) normalized by cluster mass for RXJ1716 cluster with SFRs(MIR) of other clusters in Bai et al. (2007) (i.e. originally from MIR surveys by Bai et al. 2006 for Coma, Biviano et al. 2004 for A2218, Duc et al. 2002 for A1689, Coia et al. 2005a for A2219, Coia et al. 2005b for CL0024, Marcillac et al. 2007 for RXJ0152 and Bai et al. 2007 for MS1054). We also add three more recently reported data points at $z = 0.06$ (A3266) from Bai et al. (2009), at $z = 0.08$ (A2255) from Shim et al. (2009) and at $z = 1$ as a composite value of three $z \sim 1$ clusters presented in Krick et al. (2009). We use M_{200} as the cluster mass for RXJ1716 (same as in Section 8.1), but the trend does not change if we use a lensing mass of $2.6 \pm 0.9 h^{-1} \times 10^{14} M_{\odot}$ (Clowe et al. 1998) to be consistent with Bai et al. (2007) who mainly use lensing masses. We can see a similar evolutionary trend with redshift following $\propto (1+z)^6$ in cluster star-forming activity to that seen in Fig. 14.

On the other hand, many field studies showed that the cosmic star formation rate density or SSFR of field galaxies decline since $z \sim 1$ following $\propto (1+z)^3$ (e.g. Hopkins 2004; Yoshida et al. 2006). The difference in the power index between cluster and field suggests that the galaxy evolution in cluster environment is accelerated compared to that in the general field since $z \sim 1$ (see also Kodama & Bower 2001), although we need a larger sample of distant clusters to confirm this interesting result and to quantify environmental effects.

It would be expected that the number (or fraction) of actively star-forming galaxies and the relative importance of hidden star-formation may increase with redshift. The combined approach of deep H α and MIR observations for $z \gg 1$ clusters is thus essential and it will enable us to quantify the importance of hidden side of star formation activity in clusters and its evolution.

9 SUMMARY

We conducted a narrow-band H α imaging survey for the RXJ1716 cluster at $z = 0.81$ with MOIRCS on the Subaru Telescope. This is the first wide-field H α emitter survey for $z \gtrsim 0.8$ clusters to date, and we neatly covered the pre-defined filamentary large-scale structures in and around this cluster. Combining with the wide-field MIR imaging data taken with AKARI satellite, we mapped out not only normal star-forming galaxies but also dusty starbursting galaxies across a wide range in environment. Our findings are summarized as follows:

(i) The spatial distribution of the H α emitters are very similar to that of the MIR galaxies. We find that the H α emitters avoid cluster central region ($R_c \lesssim 0.25 \text{ Mpc}$) just as the MIR galaxies do, and that the fraction of H α emitters is higher in the lower-density environment.

(ii) H α emission lines are detected mainly from blue galaxies, while the MIR galaxies tend to be redder. There are some MIR galaxies on the red sequence, and interestingly, such red

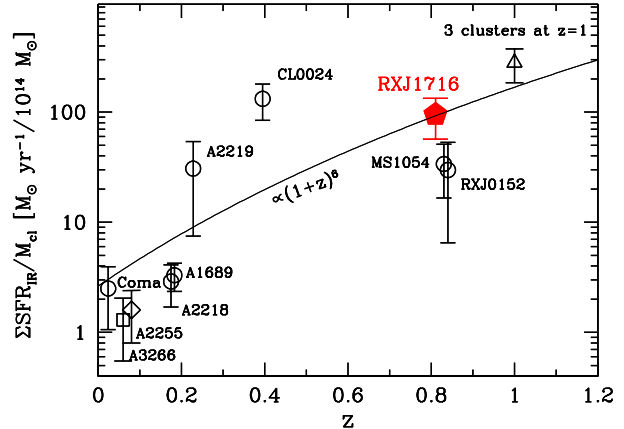


Figure 16. The integrated total cluster SFR(IR) per unit cluster mass as a function of redshift. The open circles are taken from Bai et al. (2007). The open square and the diamond are from Bai et al. (2009) and Shim et al. (2009), respectively. The open triangle shows the composite value of 3 clusters at $z = 1$ in Krick et al. (2009). For RXJ1716, we combine the H α data and the MIR data to derive the total SFR (see text).

MIR galaxies are most commonly seen in the ‘medium-density’ environment such as cluster outskirts, groups and filaments. We also find that the MIR galaxies are *not* strong H α emitters. Also, there are some MIR galaxies without detectable H α emission lines ($\text{EW} \lesssim 30 \text{ \AA}$). These suggest the existence of large amount of highly obscured galaxies in the distant cluster environment. However, we still need spectroscopic confirmation of membership of the individual MIR and H α sources to prove this interesting result.

(iii) We find some H α emitters on the red sequence. Although such population is rare (only 6 in total), these red H α emitters are concentrated in the medium-density environment, similar to the spatial distribution of MIR sources. We also find that many of the red H α emitters (4 out of 6) are detected in MIR. This suggests that such red emitters are not just gradually truncating their star-forming activity but actively star-forming with heavy dust obscuration.

(iv) We examined the amount of hidden star formation based on the ratio of SFR(IR)/SFR(H α) for the MIR galaxies. We find that for moderately star-forming galaxies with $\text{SFR(IR)} \lesssim 10 M_{\odot}/\text{yr}$ the amount of extinction for H α is ~ 1 mag, in excellent agreement with local spirals. However, for actively star-forming galaxies with $\text{SFR(IR)} \gtrsim 20 M_{\odot}/\text{yr}$, H α lines are more heavily attenuated and the extinction can exceed $A_{\text{H}\alpha} \sim 3$ in the extreme cases. Interestingly, most of such very dusty galaxies are located in the medium-density environment, suggesting the enhancement of star formation activity in such environment, most likely triggered by galaxy-galaxy interactions and/or mergers.

(v) Combining our unique H α and MIR data, we derive total SFR in the cluster down to $\sim 2 M_{\odot}/\text{yr}$ within $0.5 \times R_{200}$ from the cluster centre. We find that the cluster total SFR based on H α alone can be underestimated about factor $\gtrsim 2$ even after 1-mag extinction correction. We suggest that the mass-normalized cluster SFR evolves with redshift following $\propto (1+z)^6$, although the number of clusters studied so far is still small. We need a much larger sample of clusters studied in MIR and should go back to more distant

clusters at the same time, to fully understand the evolution of star-forming activity in clusters.

Overall, we have stressed the importance of cluster outskirts as a key environment for galaxy transition. Our results also imply that we need to be very careful when studying star formation activity in distant clusters. We may miss a significant amount of star formation if we have only optical information (even with the H α line), in particular in the cluster outskirts where starbursting populations are seen. In order to trace the true star formation activity in distant clusters, MIR-FIR observations will be essential on top of the optical-NIR observations.

ACKNOWLEDGMENT

We thank the anonymous referee for the careful reading of the paper and for helpful suggestions, which improved the paper. We thank Dr. Hyunjin Shim and Dr. Myungshin Im for kindly providing us their data for A2255. The optical and NIR data used in this paper are collected at the Subaru Telescope, which is operated by the National Astronomical Observatory of Japan (NAOJ). We acknowledge Dr. Masami Ouchi and Dr. Ryuji Suzuki for their great contribution to designing the NB119 filter on MOIRCS. The mid-infrared data that we used in this study are based on observations with AKARI, a JAXA project with the participation with ESA. This work was financially supported in part by a Grant-in-Aid for the Scientific Research (Nos. 18684004; 21340045) by the Japanese Ministry of Education, Culture, Sports and Science. Y.K. and M.H. acknowledge support from the Japan Society for the Promotion of Science (JSPS) through JSPS research fellowships for Young Scientists.

REFERENCES

- Bai L., Rieke G. H., Rieke M. J., Hinz J. L., Kelly D. M., Blaylock M., 2006, *ApJ*, 639, 827
- Bai L., et al., 2007, *ApJ*, 664, 181
- Bai L., Rieke G. H., Rieke M. J., Christlein D., Zabludoff A. I., 2009, *ApJ*, 693, 1840
- Balogh M., et al., 2004, *MNRAS*, 348, 1355
- Balogh M. L., Couch W. J., Smail I., Bower R. G., Glazebrook K., 2002, *MNRAS*, 335, 10
- Balogh M. L., Morris S. L., 2000, *MNRAS*, 318, 703
- Bavouzet N., Dole H., Le Floc'h E., Caputi K. I., Lagache G., Kochanek C. S., 2008, *A&A*, 479, 83
- Bertin E., Arnouts S., 1996, *A&AS*, 117, 393
- Biviano A., et al., 2004, *A&A*, 425, 33
- Butcher H., Oemler A., Jr., 1984, *ApJ*, 285, 426
- Calzetti D., Armus L., Bohlin R. C., Kinney A. L., Koornneef J., Storchi-Bergmann T., 2000, *ApJ*, 533, 682
- Caputi K. I., et al., 2007, *ApJ*, 660, 97
- Chary R., Elbaz D., 2001, *ApJ*, 556, 562
- Clowe D., Luppino G. A., Kaiser N., Henry J. P., Gioia I. M., 1998, *ApJ*, 497, L61
- Coia D., et al., 2005, *A&A*, 431, 433
- Coia D., et al., 2005, *A&A*, 430, 59
- Couch W. J., Balogh M. L., Bower R. G., Smail I., Glazebrook K., Taylor M., 2001, *ApJ*, 549, 820
- Dopita M. A., Pereira M., Kewley L. J., Capaccioni M., 2002, *ApJS*, 143, 47
- Dressler A., 1980, *ApJ*, 236, 351
- Dressler A., et al., 1997, *ApJ*, 490, 577
- Dressler A., Smail I., Poggianti B. M., Butcher H., Couch W. J., Ellis R. S., Oemler A. J., 1999, *ApJS*, 122, 51
- Dressler A., Rigby J., Oemler A., Fritz J., Poggianti B. M., Rieke G., Bai L., 2009, *ApJ*, 693, 140
- Duc P.-A., et al., 2002, *A&A*, 382, 60
- Ettori S., Tozzi P., Borgani S., Rosati P., 2004, *A&A*, 417, 13
- Fadda D., Biviano A., Marleau F. R., Storrie-Lombardi L. J., Durret F., 2008, *ApJ*, 672, L9
- Finn R. A., et al., 2005, *ApJ*, 630, 206
- Finn R. A., Zaritsky D., McCarthy D. W., Jr., 2004, *ApJ*, 604, 141
- Gallazzi A., et al., 2009, *ApJ*, 690, 1883
- Garn T., et al., 2009, *MNRAS* in press, arXiv:0911.2511
- Geach J. E., et al., 2006, *ApJ*, 649, 661
- Gioia I. M., Henry J. P., Mullis C. R., Ebeling H., Wolter A., 1999, *AJ*, 117, 2608
- Gómez P. L., et al., 2003, *ApJ*, 584, 210
- Goto T., Yamauchi C., Fujita Y., Okamura S., Sekiguchi M., Smail I., Bernardi M., Gomez P. L., 2003, *MNRAS*, 346, 601
- Haines C. P., Smith G. P., Egami E., Okabe N., Takada M., Ellis R. S., Moran S. M., Umetsu K., 2009, *MNRAS*, 396, 1297
- Haines C. P., et al., 2009, *ApJ*, 704, 126
- Hayashi M., Kodama T., Koyama Y., Tanaka I., Shimasaku K., Okamura S., 2009, *MNRAS* in press, arXiv:0911.2530
- Henry J. P., et al., 1997, *AJ*, 114, 1293
- Homeier N. L., et al., 2005, *ApJ*, 621, 651
- Hopkins A. M., 2004, *ApJ*, 615, 209
- Ichikawa T., et al., 2006, *SPIE*, 6269,
- Iye M. et al. 2004, *PASJ*, 56, 381
- Jarrett T. H., Chester T., Cutri R., Schneider S., Skrutskie M., Huchra J. P., 2000, *AJ*, 119, 2498
- Jeltema T. E., Canizares C. R., Bautz M. W., Buote D. A., 2005, *ApJ*, 624, 606
- Kennicutt R. C., Jr., 1998, *ARA&A*, 36, 189
- Kennicutt R. C., Jr., Tamblyn P., Congdon C. E., 1994, *ApJ*, 435, 22
- Kodama T., Bell E. F., Bower R. G., 1999, *MNRAS*, 302, 152
- Kodama T., & Bower, R. G., 2001, *MNRAS*, 321, 18
- Kodama T., Smail I., Nakata F., Okamura S., Bower R. G., 2001, *ApJ*, 562, L9
- Kodama T., Balogh M. L., Smail I., Bower R. G., Nakata F., 2004, *MNRAS*, 354, 1103
- Kodama T., et al., 2005, *PASJ*, 57, 309
- Koyama Y., Kodama T., Tanaka M., Shimasaku K., Okamura S., 2007, *MNRAS*, 382, 1719
- Koyama Y., et al., 2008, *MNRAS*, 391, 1758
- Krick J. E., Surace J. A., Thompson D., Ashby M. L. N., Hora J. L., Gorjian V., Yan L., 2009, *ApJ*, 700, 123
- Lagache G., et al., 2004, *ApJS*, 154, 112
- Lewis I., et al., 2002, *MNRAS*, 334, 673
- Marcillac D., Rigby J. R., Rieke G. H., Kelly D. M., 2007, *ApJ*, 654, 825
- Martini P., Kelson D. D., Mulchaey J. S., Trager S. C., 2002, *ApJ*, 576, L109
- Miyazaki S., et al., 2002, *PASJ*, 54, 833
- Murakami H., et al., 2007, *PASJ*, 59, 369
- Onaka T., et al., 2007, *PASJ*, 59, 401
- Ouchi M., et al., 2004, *ApJ*, 611, 660
- Poggianti B. M., Wu H., 2000, *ApJ*, 529, 157
- Poggianti B. M., et al., 2006, *ApJ*, 642, 188
- Postman M., et al., 2005, *ApJ*, 623, 721
- Postman M., Geller M. J., 1984, *ApJ*, 281, 95

- Puget J. L., Leger A., 1989, *ARA&A*, 27, 161
Pozzetti L., Mannucci F., 2000, *MNRAS*, 317, L17
Saintonge A., Tran K.-V. H., Holden B. P., 2008, *ApJ*, 685, L113
Schlegel D. J., Finkbeiner D. P., Davis M., 1998, *ApJ*, 500, 525
Shim H., et al., 2009, *ApJ*, submitted
Smail I., Morrison G., Gray M. E., Owen F. N., Ivison R. J., Kneib J.-P., Ellis R. S., 1999, *ApJ*, 525, 609
Sobral D., et al., 2009, *MNRAS*, 398, 75
Suzuki R., et al., 2008, *PASJ*, 60, 1347
Tanaka M., Goto T., Okamura S., Shimasaku K., Brinkmann J., 2004, *AJ*, 128, 2677
Tanaka M., Kodama T., Arimoto N., Okamura S., Umetsu K., Shimasaku K., Tanaka I., Yamada T., 2005, *MNRAS*, 362, 268
Tran K.-V. H., Saintonge A., Moustakas J., Bai L., Gonzalez A. H., Holden B. P., Zaritsky D., Kautsch S. J., 2009, *ApJ*, 705, 809
Tresse L., Maddox S., Loveday J., Singleton C., 1999, *MNRAS*, 310, 262
Wolf C., Gray M. E., Meisenheimer K., 2005, *A&A*, 443, 435
Yagi M., Kashikawa N., Sekiguchi M., Doi M., Yasuda N., Shimasaku K., Okamura S., 2002, *AJ*, 123, 66
Yoshida M., et al., 2006, *ApJ*, 653, 988